Interdiffusion at Homopolymer/Random Copolymer Interfaces Investigated by Energy-Filtering Transmission Electron Microscopy

Yonggui Liao, Ayumi Nakagawa, and Shin Horiuchi*

Nanotechnology Research Institute, National Institute of Advanced Industrial Science and Technology (AIST), 1-1-1, Higashi, Tsukuba, Ibaraki 305-8565, Japan

Toshiaki Ougizawa

Department of Organic and Polymeric Materials, Tokyo Institute of Technology, 2-12-1, Ookayama, Meguro-ku, Tokyo 152-8550, Japan

Received July 11, 2007; Revised Manuscript Received August 27, 2007

ABSTRACT: Interdiffusion and welding behaviors of a miscible pair of poly(methyl methacrylate)/poly(styrene-*ran*-acrylonitrile) (PMMA/SAN) laminates were investigated by energy-filtering transmission electron microscopy (EFTEM) and asymmetric double beam cantilever (ADBC) test. The composition variations across the interfaces were investigated using oxygen and nitrogen elemental maps and by electron energy loss spectroscopy. The composition profiles exhibited two-step gradients with a minimum gradient at the midpoint of the interfacial region. Welding experiments by ADBC test also showed an unusual toughness−thickness relationship where the toughness continued to increase even in the interfacial regions that are significantly thicker than the size of entanglement spacing. Both EFTEM analysis and ADBC test indicated that during the interdiffusion process the interfacial layer develops into entanglement structures that are mechanically more stable. The combination of EFTEM and ADBC tests provided us with a better understanding of the interfacial structures including entanglements.

Introduction

Polymer interdiffusion is of significant importance both for fundamental studies[1−3] and for practical applications such as adhesion, welding, coating, and laminating of films. The performances of these applications are closely related to the entanglement structures within the interfacial layer that are formed via interchain penetration during the interdiffusion process. The entanglement structure of polymers is known to be one of the several kinds of fundamental structures of polymer materials. However, detailed topological picture of the entanglement structure is so difficult to obtain experimentally, and hence it is not yet fully understood. Especially, the local entanglement structures formed via interdiffusion of polymers have been difficult to characterize.

Many experimental techniques, such as Rutherford backscattering spectrometry (RBS),[4,5] forward recoil spectrometry (FRES),[6−12] neutron reflection (NR),[13−17] nuclear reaction analysis (NRA),[13,18−20] rheometry,[21,22] ellipsometry,[16,23−26] X-ray reflectometry (XR),[27,28] fluorescence spectroscopy (FS),[29,30] dynamic light scattering (LS),[31] positron annihilation lifetime spectroscopy (PALS),[32] nuclear magnetic resonance spectroscopy (NMR),[6,33,34] infrared spectroscopy (IR),[6,35−37] Raman spectroscopy,[38−41] secondary ion mass spectroscopy (SIMS),[13,27,42−47] transmission electron microscopy (TEM),[23] and scanning transmission electron microscopy (STEM),[48,49] have been employed for the study of polymer interdiffusion. But, RBS, FRES, NR, and NRA cannot measure concentration profiles directly, and therefore deuterated samples (or special preprocessing) are necessary for their evaluation, although these techniques have high resolution on a scale of angstroms. On the other hand, in order to obtain corresponding concentration profiles, some assumptions have to be made for rheometry, FS, ellipsometry, XR, LS, and PALS. IR and Raman spectroscopies are limited by a depth resolution of 0.1−1 μm, although they can provide useful information at large interdiffusion depths. And moreover, SIMS can directly measure the concentration profile with high resolution of 10 nm, but it is required that the top layer be planar and of uniform thickness. The conventional TEM and STEM usually require specimens to be stained with heavy metals for profiling the concentration. This staining process, however, may also lose the original structure, and therefore a technique with advantages of high spatial resolution, real space observation, and nontoxic preprocessing and a technique with no limitation regarding specimen geometry could quite promising for the study of polymer interdiffusion.

Energy-filtering transmission electron microscopy (EFTEM) allows us to characterize interfacial structures in samples of any shape without the use of heavy metal staining. In our previous work[53] we had explored the changes in the interfacial structures and the adhesion strength of poly(methyl methacrylate)/poly(styrene-*ran*-acrylonitrile) (PMMA/SAN) laminates when the AN (acrylonitrile) content in SAN was varied by employing the EFTEM and asymmetric double beam cantilever (ADBC) test. In that work the concentration profiles were obtained by the pixel intensity profiles across the interface on the elemental maps without the use of any mathematical approximation. The ADBC test was frequently employed for the evaluation of interfacial toughness because it provided us with valuable information on the interfacial characteristics in terms of the adhesion strength and the fracture behavior of interfaces. Here in this paper we report on our continued studies on the subject by investigating the interfacial structures formed by the interdiffusion of a miscible polymer pair by the EFTEM and ADBC test.

* Corresponding author: Tel +81-29-861-6281; Fax +81-29-861-4773; e-mail s.horiuchi@aist.go.jp.

10.1021/ma071535g CCC: $37.00
Published on Web 10/02/2007

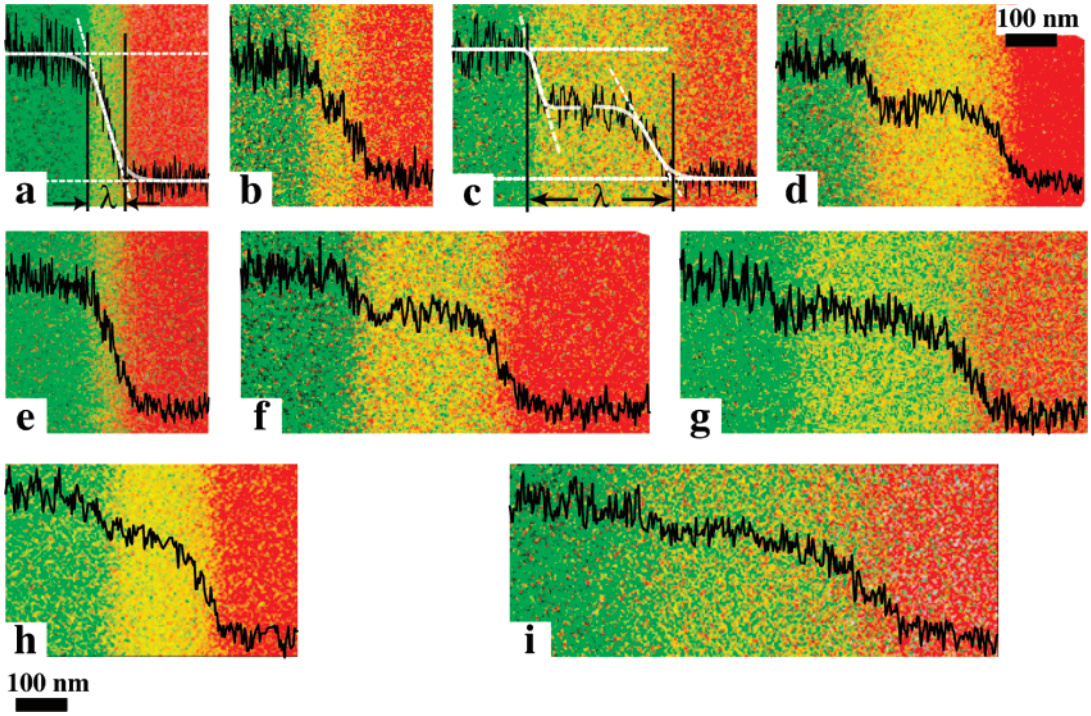

Figure 1. RGB composite images of the oxygen (green) and the nitrogen (red) maps of PMMA/SAN laminates annealed at 130 °C for 1 (a), 4 (b), 12 (c), and 24 h (d); at 140 °C for 1 (e), 4 (f), and 8 h (g); and at 150 °C (h) and 160 °C (i) for 2 h. All the images are shown at the same magnifications. The ratio of the oxygen to nitrogen concentration profiles across the interfaces is overlapped onto the corresponding images. (a) and (c) present the procedure to determine the interface width (λ) by fitting the profiles with hyperbolic tangent function.

Experimental Section

Materials and Sample Preparation. PMMA (M_w 113 kg/mol, $M_w/M_n = 2.1$, modulus 3743 MPa; Wako Chemical Co. Ltd., Japan) and SAN with the acrylonitrile content of 29 wt % (SAN, M_w 213 kg/mol, $M_w/M_n = 3.3$, modulus 4123 MPa) were used without any further purification. The glass transition temperatures (T_g) of PMMA and SAN, measured with a differential scanning calorimeter (Perkin-Elmer DSC 7) at a heating rate of 10 °C/min, were 98 and 105 °C, respectively. PMMA and SAN were compression-molded into sheets between silicon wafers at 180 °C. The sheet specimens with 50 × 8.5 mm were laminated at 130, 140, 150, and 160 °C for various times in air under slight pressure to ensure proper contact between the two surfaces.

Measurements of Interfacial Toughness (G_c). The interfacial adhesion strength of PMMA/SAN interfaces was evaluated by the ADBC test. A detailed procedure and the effectiveness of this method for the evaluation of interface toughness have been described elsewhere.[54−56] After annealing, the laminates were quenched to room temperature to freeze interdiffusion. A razor blade with a thickness (d) of 2.0 mm was then driven into the interface between the two polymer sheets to propagate a crack along the interface. When the crack propagation stopped, the length ahead of the blade was measured under a microscope. The interfacial toughness, G_c, was then calculated using the following equation:

$$G_c = \frac{3d^2 E_1 h_1^3 E_2 h_2^3}{8a^4} \frac{E_1 h_1^3 C_2^2 + E_2 h_2^3 C_1^2}{[E_1 h_1^3 C_2^3 + E_2 h_2^3 C_1^3]^2} \qquad (1)$$

where $C_i = 1 + 0.64(h_i/a)$, E_i is the modulus, and h_i is the thickness of beam i. A proper thickness ratio of PMMA and SAN sheets was found at 1.8 and 1.7 mm, respectively, to give a minimum G_c value.

EFTEM. The laminates were microtomed perpendicular to the interface to obtain sections with a thickness of 50 nm. For focus adjustment during TEM operation and the drift correction for element mapping, gold nanoparticles (diameter ~ 10 nm) were dispersed onto thin sections using a dilute gold colloid aqueous solution. Elemental mapping and electron energy loss spectroscopy (EELS) were carried out using a LEO922 in-column energy-filtering transmission electron microscope (EFTEM, Carl Zeiss SMT, Germany) equipped with an Omega-type energy filter at an accelerating voltage of 200 keV. To minimize the radiation damage to the specimens from the electron beam, all observations were carried out cryogenically at −160 °C. Elemental mapping and electron energy loss spectroscopy (EELS) were carried out by Image EELS technique as was described in detail in our previous papers.[50,51,53,57] A series of energy-filtered images with the energy width of 5 eV were acquired with the energy increment of 4 eV in the energy loss range from 370 to 590 eV. Nitrogen and oxygen elemental maps were created by the "two-window jump ratio" method. In this method, the post-edge image, corresponding to the energy-filtered image beyond the ionization edge of a element, was divided by the pre-edge image, corresponding to the energy-filtered image below the ionization of the element of interest.[51] The nitrogen and oxygen ionization edges were found at 400 and 535 eV, respectively. Here, two recorded images among the stack of the images acquired by Image EELS were selected and used for the mapping of the element of interest.

Parallel EELS was also employed for recording EELS spectra.[58] Specimen area to be analyzed was determined by inserting an aperture at the entrance of the filter. The spectrum was then imaged on a slow scan CCD camera, and an image analysis system measured the intensity and converted it into a spectrum. Specimen thickness for this measurement was measured by ellipsometry using a spectroscopic ellipsometer (M-220, JASCO Co., Ltd., Japan).

Results and Discussion

Interdiffusion Behaviors Investigated by EFTEM. The interfaces formed via diffusion of PMMA and SAN were imaged and the composition profiles of the interfaces were created by the method reported in our previous work.[53] Figure 1 shows RGB composite images of the oxygen (green) and the nitrogen (red) elemental maps that exhibits the interfacial regions as yellow layers due to the composition of the red and green pixels. The composition profiles were created by calculating the ratio of the intensity profiles across the interface of the two elemental

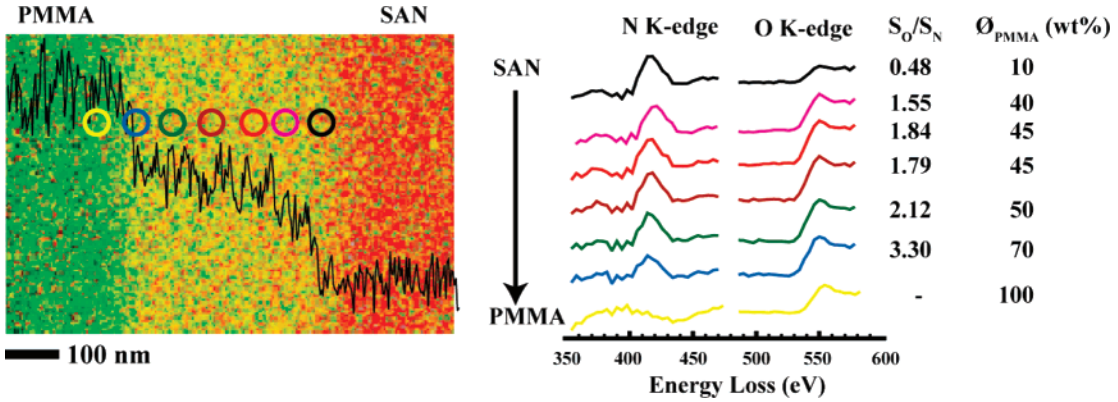

Figure 2. Changes in the N and O K-edges across the interface of PMMA/SAN laminate annealed at 130 °C for 12 h. The background intensities were subtracted in accordance with the exponential law. The analyzed positions are indicated in the image with the same colors of the spectra. Ratios of the integrated intensities (S_O/S_N) and the estimated PMMA compositions (ϕ_{PMMA}) are also indicated.

maps. Figure 1 shows the growth of the interfacial layer with welding time at temperatures higher than the glass transition temperatures (T_gs) of both polymers. The composition profiles across the interfaces welded for the short periods at the relatively lower temperatures (Figure 1a,b,e) show smooth single gradients, which could be well fitted by a hyperbolic tangent function proposed for the description of the concentration profiles of polymer blends.[23] On the other hand, with increasing welding time the interfacial zones gradually became wider and the profiles resulted in two-step gradients in the interfacial regions where it exhibited a plateau in the middle part of the interfacial region. It seems that the layer of PMMA/SAN blend resulting in an equivalent composition was formed at the middle part of the region during the interdiffusion process. This layer appeared after 12 h at 130 °C (Figure 1c), while at 140 °C it appeared only after 4 h (Figure 1f). The higher temperature accelerated not only the diffusion but also the formation of this layer. At the temperatures sufficiently higher than the T_gs of both polymers (150 and 160 °C), the composition profiles with the minimum gradients at the midpoint were obtained in the earlier periods of the diffusion (Figure 1, parts h and i, respectively), indicating that the composition profiles were obtained by mutual diffusion and not by the swelling of a polymer into the other.

The variation of the composition across the interface can also be estimated by the intensity ratios of the core-loss peaks of EELS spectra at the points of interest in the image.[51] Figure 2 shows the changes in the intensities of the nitrogen and oxygen core-loss peaks across the interface in the sample welded at 130 °C for 12 h, where the analyzed regions are indicated in the image. The ratios of the integrated areas under the oxygen core-loss peak with the energy window of 60 eV against that of the nitrogen (S_O/S_N) were calculated, and the values thus obtained are indicated therein. We could confirm that the ratios of the integrated intensities of the core-loss peaks are almost constant around the region having the minimum composition gradient.

Atomic ratios of the two elements can be calculated using the integrated intensities of the core-loss peaks (S_i) in an EELS spectrum using the following equation

$$\frac{N_1}{N_2} = \frac{S_1(\Delta,\alpha)}{S_2(\Delta,\alpha)} \frac{\sigma_2(\Delta,\alpha)}{\sigma_1(\Delta,\alpha)} \qquad (2)$$

where σ_i is inelastic partial cross section, Δ is energy window, and α is collection angle. In order to obtain true atomic ratios, σ_x has to be correctly determined, and the signal intensity contributed by the ionization of an element has to be calculated

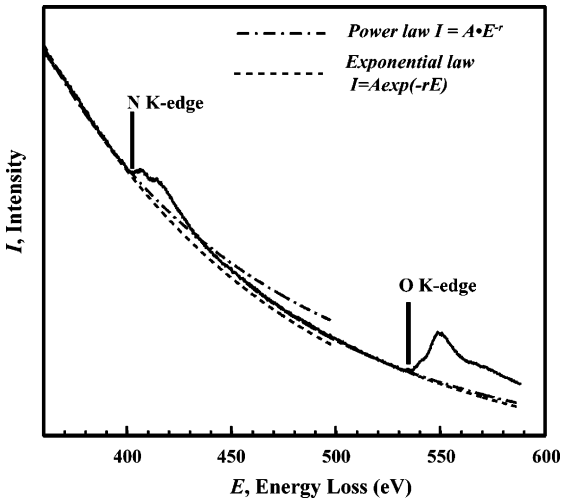

Figure 3. Parallel EELS spectrum acquired in a miscible PMMA/SAN (60/40 by weight) blend film with 50 nm thickness with the background fitting curves for the nitrogen and oxygen K-edges using exponential and power models.

accurately by the fitting of background intensities. However, the difficulty in the determination of σ_x and the inaccuracy of the background fitting for the calculation of the integrated core-loss signals frequently cause an uncertainty in the quantitative analysis in EELS. Figure 3 shows an EELS spectra acquired from a PMMA/SAN (60/40 by weight) miscible blend film by means of parallel EELS in the energy loss range from 360 to 580 eV, including both the nitrogen and oxygen ionization edges at 395 and 535 eV, respectively. It also shows the background fittings by extrapolating the background using a power-law function of the form $I = AE^{-r}$ and exponential function of the form $I = A\exp(-rE)$, where I is the signal intensity, E is the energy loss values, and A and r are the fitting parameters. There is often a degree of uncertainty in the fitting, especially in the fitting of the nitrogen core-loss peak because the large core-loss peak of carbon with the ionization edge at 285 eV appears just below the nitrogen ionization where it frequently impedes the detection of nitrogen and influences the background intensities. This situation makes it difficult to fit the background appropriately for the removal of the background intensity. As shown in Figure 3, the background fitting by the two models gave different results for the nitrogen core-loss peak, whereas the oxygen core-loss peak can be well fitted by the two models. Therefore, the integrated intensity of the nitrogen core-loss peak may not represent the true number of atoms in the measured area. In order to avoid this problem, the ratios of the core-loss

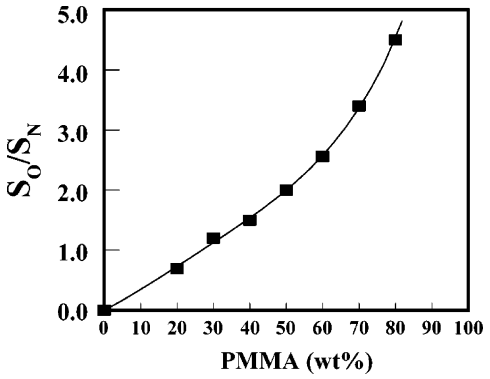

Figure 4. Ratio of the integrated intensities of N and O core-loss peaks (S_O/S_N) vs the PMMA composition in blend films of PMMA/SAN by parallel EELS. The integrated intensities were estimated by using exponential power fitting.

peaks of oxygen and of nitrogen (S_O/S_N) were experimentally measured using PMMA/SAN homogeneous blend films with known compositions by the parallel EELS, and then a master curve presenting the PMMA/SAN composition dependence of the ratio of the integrated intensity of the core-loss peaks was created, as shown in Figure 4. The spectra were acquired under the same conditions as for the acquisition of the series of the images for the creation of the elemental maps and EELS analysis. That is, the beam with the intensity of 3.5×10^4 EL/(nm^2 s) was irradiated on the specimen for 5 s for 60 times at the magnification of 31 500 at −160 °C, corresponding to the dose of 168 C/cm^2. Specimen thickness was adjusted at 50 nm by spin-coating using a THF solution onto a cleaved NaCl single crystal. Then, we could estimate the approximate compositions (ϕ_{PMMA}) in the interfacial region as shown in Figure 2, indicating that the middle part in the interface with the low composition gradient contained PMMA at 40−50 wt %. In the other samples, the compositions along the low gradient profile were also estimated in the comparable levels.

The interdiffusion of PMMA/SAN at the temperatures above T_gs of both polymers exhibits unusual composition profiles that differ from the classical Fick's law profile where the diffusion coefficient is constant and the composition gradient is maximum at the profile midpoint. It has been known that such an unusual composition profile is obtained when interdiffusion between two polymers undergoes a thermodynamic "acceleration". In this case, the mixing is promoted by attractive interactions between the different segments, which greatly accelerate the interdiffusion process as compared to the self-diffusion. The attractive interactions is proportional to $\chi\upsilon(1 - \upsilon)$, where χ is Flory−Huggins interaction parameter and υ is the volume fraction of one polymer, and the diffusion coefficient $D_m(\upsilon)$ is composition dependent with a maximum around $\upsilon = 0.5$. $D_m(\upsilon)$ can be expressed from the analysis of Flory−Huggins theory for the free energy of mixing of a polymer blend[3]

$$D_m(\upsilon) = D_0[1 - 2\chi N\upsilon(1 - \upsilon)] \quad (3)$$

where D_0 is a coefficient expressing the mobility of the components (note: if the two materials have identical mobility, this would correspond to their self-diffusion coefficient). If the absolute value of χ is about an order larger than $1/N$, where N is the polymerization index for PMMA or SAN, the second term in eq 3, i.e., the enthalpy term, dominates for all but the smallest concentrations. It leads to a thermodynamic "acceleration" diffusion behavior with a strong concentration dependent mutual diffusion coefficient D_m with a much higher diffusion constant in the middle of the concentration range.[17]

An example of this effect was exhibited by a polymer pair of poly(vinyl chloride)/poly(ϵ-caprolactone) (PVC/PCL).[49] This pair has a large negative χ parameter (−0.38), and thus the mutual diffusion coefficient D_m becomes strongly composition dependent, and thus much higher diffusion constants can be obtained in the middle concentration range.[17] Therefore, the interdiffusion is accelerated in the midpoint in the interfacial zone, which leads to the formation of an interfacial region with the equivalent composition.

The interaction parameter between PMMA and SAN can be calculated from the following equation[60]

$$\chi = \beta\chi_{S/MMA} + (1 - \beta)\chi_{AN/MMA} - \beta(1 - \beta)\chi_{S/AN} \quad (4)$$

where $\chi_{i/j}$ is segmental interaction parameter which can be obtained from the literature[25] and β is the mole fraction of styrene in SAN. χ is calculated as −0.021, −0.028, −0.028, and −0.012 at 130, 140, 150, and 160 °C, respectively. The χ parameters are not as high as that of PVC/PCL but are still significantly higher than $1/N$. Thus, one of the main reasons for our case is assumed to be thermodynamic "acceleration".

While studying the interface between polycarbonate (PC) and the blend of SANs with different AN contents by SIMS, Schaffer and co-workers found a profile having a plateau part. In that case, the SAN with a lower AN content (17 wt %) in the mixture preferentially segregates into the PC side because it was more compatible with PC than the SAN with higher AN content (31 wt %).[43] SAN is a random copolymer, and it has a chemical distribution with respect to the copolymer composition. Some parts of the copolymer may be within the miscibility window with PMMA and others not. As a result, more compatible moieties in SAN move to the interface.[43] However, SAN with different compositions were not intensively added in this study, and thus the chemical distribution of the SAN copolymer is not considered to be a major reason for the unusual profiles.

Interfacial Width (λ), Mutual Diffusion Coefficient (D_m), and Apparent Activation Energy (E_a). Compared with the rate of diffusion and that of segmental relaxation, the polymer interdiffusion can be usually divided into two cases, i.e., the normal Fickian diffusion and the case II diffusion.[42] Case I is the normal Fickian diffusion, where the rate of diffusion is much less than that of segmental relaxation, such as liquid−liquid interdiffusion. This diffusion can be well described by reptation model proposed by Edwards[1] and de Gennes.[2] In this model, the movement of a polymer chain is constrained in a virtual tube composed by the entanglement network of the surrounding chains. The chains move by a Rouse-type motion[61] along their contour within this tube. For time longer than the reptation time, normal Fickian diffusion is obeyed with[3]

$$\lambda = 2(D_m t)^{1/2} \quad (5)$$

On the contrary, for case II diffusion, the diffusion rate is more rapid than the segmental relaxation. For instance, for a liquid/glassy polymer pairs, the diffusion is controlled by the time-dependent mechanical response of the polymer to the osmotic swelling stress at the penetrant diffusion front, which constitutes the central aspect of the case II diffusion with a scaling of the interfacial width $\lambda \sim t$.

In our case, the interfacial width was calculated from the profile with the aid of the fitted curve. The tangent was drawn at the inflection point of the fitting curves creating a so-called wedge shape, and then the interfacial width (λ) was defined as shown in Figure 1a. For a composition profile with a middle

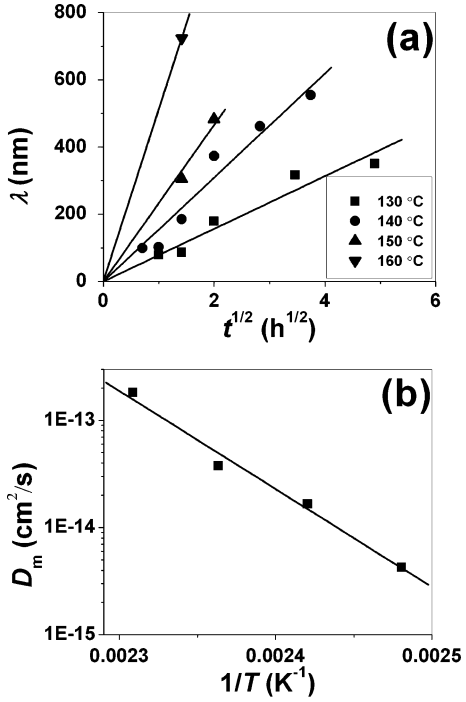

Figure 5. (a) Interfacial width (λ) vs square root of diffusion time for PMMA/SAN interfaces annealed at 130 °C (squares), 140 °C (circles), 150 °C (up triangles), and 160 °C (down triangles). (b) Semilogarithmic plot of mutual diffusion coefficient (D_m) as a function of 1/T. The solid line represents the best fit of an Arrhenius equation to the data giving the apparent activation energy, $E_a = 175 \pm 15$ kJ/mol.

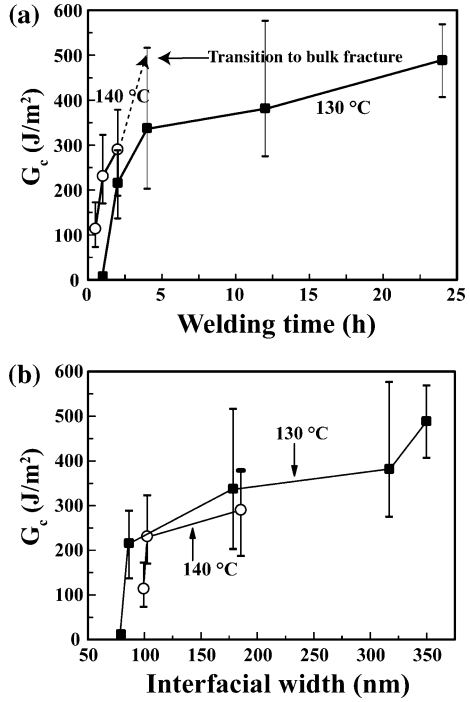

Figure 6. (a) Interfacial fracture toughness (G_c) vs welding time and (b) G_c vs interface width of PMMA/SAN laminates annealed at 130 °C (solid squares) and 140 °C (open circles).

plateau part, the profile was separated into two single hyperbolic tangent shapes and was individually fitted by the function, as shown in Figure 1c. Figure 5a shows the λ grows linearly with the square root of the welding time, $t^{1/2}$. In this case, although the local diffusion driven by a thermodynamic "acceleration" mechanism leads to an "anti-Fickian" profile, the overall interdiffusion seems not to obey a case II diffusion with a scaling of $\lambda \sim t$ but to obey the Fikian diffusion.[3] The apparent D_m can be calculated using the eq 5, which gives 4.26×10^{-15}, 1.66×10^{-14}, 3.76×10^{-14}, and 1.82×10^{-13} cm^2/s at 130, 140, 150, and 160 °C, respectively. The solid line in Figure 5b represents the best fit of an Arrhenius expression to the data, calculating the apparent activation energy, E_a, as 175 ± 15 kJ/mol.

$$D_m = D_0 \exp(E_a/RT) \tag{6}$$

To compare our results to the data reported in the literature, we here use the method proposed by Qiu and Bousmina.[21] All these four D_ms were converted into those at the reference temperature of 120 °C. The converted data were $(0.62-2.43) \times 10^{-16}$ cm^2/s, which are about 1 order of magnitude larger than those obtained by Kim et al. (1.1×10^{-17} cm^2/s)[9] using FRES and are in good agreement with the results obtained by Yukioka et al. (1.0×10^{-16} cm^2/s)[24,26] using ellipsometry and that obtained by Qiu et al. (3.7×10^{-16} cm^2/s) using rheometry.[21] These results imply that EFTEM is really a powerful technique to investigate the polymer interdiffusion.

Relationship between Interfacial Structures and Interface Toughness (G_c). In order to investigate the properties of the interfacial layers formed via interdiffusion, the developments of the welding of PMMA/SAN laminates are evaluated by ADBC test. Figure 6a shows that the interface toughness (G_c) is enhanced with the interdiffusion time at 130 and 140 °C. The mean values of at least 10 data points for each laminate are plotted together with their minimum and maximum values. X-ray photoelectron spectroscopy measurements ensured that both sides of the fracture surfaces showed nitrogen and oxygen 1s signals with comparable intensities, indicating that the crack propagates within the interfacial zone. It should be noted that when the laminate is welded at 140 °C, the crack cannot be propagated into the interface after 2 h and is kinked out of the interface, resulting in the breakage of the relatively weaker PMMA sheet. On the other hand, the G_c values can be measured up to 480 J/m^2 after 24 h at 130 °C. These results suggest that the interface toughness exceeds this value and is close to the fracture toughness of the bulk materials, ~ 500 J/m^2 for PMMA[62] or higher after 4 h at 140 °C. It should be taken into consideration that the modulus of the interfacial zone is changed from the original modulus of the bulk polymers with increase of the thickness of the interfacial layer. Thus, it is impossible to calculate the true value of G_c after the formation of thick interfaces because the true modulus with the presence of the thick interfacial layers was unknown. However, it can be seen that qualitatively the interface becomes gradually tough with increase in the welding time.

It has been known that the polymer self-diffusion shows direct correlation between G_c and interfacial width (λ).[63] Most of the increase in the toughness occurs over a relatively narrow range of λ between 9 and 12 nm, and then the toughness rapidly reaches to the comparable toughness of the bulk polymers. Polymer chains need only to interpenetrate roughly by an entanglement distance to provide an optimum adhesion. The fracture toughness then remains constant with further interdiffusion. On the other hand, in our case the diffusion of the two dissimilar polymers was more rapid than those between identical polymers owing to the fact that miscible polymer blends have additional energetic attractions, which is attributed to the negative χ parameter. The interface toughness could not reach the bulk values in the early stage and increased even though the wide interfacial zone for the full entanglement of the molecules has been established. It is suggested that even though with their thick interface the interdiffusing polymer chains are

not able to form entanglements which are mechanically as effective as in the bulk phase in the early stage of the diffusion. Figure 6b shows the relationships between G_c and λ obtained at the two welding temperatures, showing that G_c increases with increase of λ even in such a thick interfacial region. It indicates that there remained a weak plane in the interfacial region that allows the crack propagation even after the long welding periods in the laminates welded at 130 °C. The unique composition profiles across the interfaces as shown in Figure 1 resulted in the unique relationship between G_c and the interfacial width. The weakest plain in the interfacial region is probably at the edges of the interfacial region with high concentration gradients. However, those regions are much wider than the critical width (9−12 nm) for the adhesion between identical polymers.

It should be noted that the same interfacial thickness attained at the different temperatures does not give the same G_c. Figure 6b indicates that at a fixed thickness the lower temperature (130 °C) gave a higher G_c that was achieved for a longer welding period than that at the higher temperature (140 °C). It implies that the interfaces formed at high welding temperature have quite different chain topography that is far from the one in an equilibrium situation established for longer periods.

The adhesion of the laminates annealed for long periods was so high that no cracks were produced ahead of the razor blade. It is not possible, unfortunately, to estimate such high toughness quantitatively by ADBC test. However, it indicates qualitatively that the toughness of the interfaces was much higher than the bulk materials, suggesting that the interdiffusion of PMMA and SAN forms an interfacial region with entanglements that are mechanically more effective than those of the bulk polymers. The interfacial zone undergoes a gradual change toward a more entangled system with the welding time, and then the interface becomes tougher compared to the bulk polymers. What we learned from the welding experiments regarding the interfacial structures is consistent with the results of the EFTEM analysis of the interdiffusion behaviors. As discussed in the previous section, the unusual composition profiles at the interface are achieved by the thermodynamic "acceleration", suggesting that the relatively stable interfacial region with attractive interactions between the two polymers is developed in the middle part of the interface. The production of this interfacial region during the interdiffusion leads to the high toughness of the interfaces.

Conclusion

Interfacial structures formed via interdiffusion of PMMA and SAN at various temperatures above the T_gs of both polymers were investigated by EFTEM. The study revealed that the composition profile at the interface is different from the classical "Fickian profile". Elemental analysis by EELS indicated that a layer with PMMA content of 40−50 wt % was around the midpoint of the interfacial layer. This unusual interdiffusion behavior is caused mainly by the strong attractive interactions between the two polymers and is known as thermodynamic "acceleration". The interfacial width (λ) grows linearly with the square root of the welding time, $t^{1/2}$. The mutual diffusion coefficient is in good agreement with those in the literature. Welding experiments by ADBC test for investigating the interfacial toughness also showed unusual toughness−thickness relationships; it showed that the toughness continued to increase even in interfacial regions that were significantly thicker than the entanglement spacing. This suggests that during the interdiffusion process, due to the attractive interactions as indicated by EFTEM analysis, the interfacial layer develops into entanglement that are mechanically more effective.

Conventional TEM enables us only to observe the simple morphological features by heavy metal staining, while EFTEM can provide us with better understanding of the local polymer structures. Especially, it is expected that the combination of EFTEM and ADBC test is effective to investigate the interfacial structures including entanglements.

Acknowledgment. Financial support by the NEDO for "Nanostructured Polymer Project" is gratefully acknowledged. The authors also thank Dr. Z. Y. Sun from Changchun Institute of Applied Chemistry, Chinese Academy of Sciences, for useful discussions.

References and Notes

(1) Edwards, S. F. *Proc. Phys. Soc.* **1967**, *92*, 9.
(2) de Gennes, P. G. *J. Chem. Phys.* **1971**, *55*, 572.
(3) Brochard, F.; Jouffroy, J.; Levinson, P. *Macromolecules* **1983**, *16*, 1638.
(4) Composto, R. J.; Kramer, E. J. *J. Mater. Sci.* **1991**, *26*, 2815.
(5) Jablonski, E. L.; Gorga, R. E.; Narasimhan, B. *Polymer* **2003**, *44*, 729.
(6) Lodge, T. P. *Phys. Rev. Lett.* **1999**, *83*, 3218.
(7) Nealey, P. F.; Cohen, R. E.; Argon, A. S. *Macromolecules* **1993**, *26*, 1287.
(8) Composto, R. J.; Kramer, E. J. *Macromolecules* **1992**, *25*, 4167.
(9) Kim, E.; Wu, W. C.; Garrett, P. D. *Polymer* **1994**, *35*, 5706.
(10) Kim, E.; Kramer, E. J.; Osby, J. O. *Macromolecules* **1995**, *28*, 1979.
(11) Composto, R. J.; Kramer, E. J. *Polymer* **1990**, *31*, 2320.
(12) Green, P. F.; Doyle, B. L. *Macromolecules* **1987**, *20*, 2471.
(13) Stoffel, N. C.; Dai, C. A.; Kramer, E. J.; Russell, T. P.; Deline, V.; Volksen, W.; Wu, W.; Satija, S. *Macromolecules* **1996**, *29*, 6880.
(14) Sferrazza, M.; Xiao, C.; Jones, R. A. L.; Bucknall, D. G.; Webster, J.; Penfold, J. *Phys. Rev. Lett.* **1997**, *78*, 3693.
(15) Bucknall, D. G.; Butler, S. A.; Higgins, J. S. *Macromolecules* **1999**, *32*, 5453.
(16) Sauer, B. B.; Walsh, D. J. *Macromolecules* **1991**, *24*, 5948.
(17) Klein, J. *Science* **1990**, *250*, 640.
(18) Shearmur, T. E.; Clough, A. S.; Drew, D. W.; van der Grinten, M. G. D.; Jones, R. A. L. *Macromolecules* **1996**, *29*, 7269.
(19) Shearmur, T. E.; Clough, A. S.; Drew, D. W.; van der Grinten, M. G. D.; Jones, R. A. L. *Phys. Rev. E* **1997**, *55*, R3840.
(20) Clarke, N.; Colley, F. R.; Collins, S. A.; Hutchings, L. R.; Thompson, R. L. *Macromolecules* **2006**, *39*, 1290.
(21) Qiu, H.; Bousmina, M. *Macromolecules* **2000**, *33*, 6588.
(22) Bousmina, M.; Qiu, H.; Grmela, M.; Klemberg-Sapieha, J. E. *Macromolecules* **1998**, *31*, 8273.
(23) Kressler, J.; Higashida, N.; Inoue, T.; Heckmann, W.; Seitz, F. *Macromolecules* **1993**, *26*, 2090.
(24) Yukioka, S.; Nagato, K.; Inoue, T. *Polymer* **1992**, *33*, 1171.
(25) Higashida, N.; Kressler, J.; Yukioka, S.; Inoue, T. *Macromolecules* **1992**, *25*, 5259.
(26) Yukioka, S.; Inoue, T. *Polym. Commun.* **1991**, *32*, 17.
(27) Harton, S. E.; Koga, T.; Stevie, F. A.; Araki, T.; Ade, H. *Macromolecules* **2005**, *38*, 10511.
(28) Hüttenbach, S.; Stamm, M.; Reiter, G.; Foster, M. *Langmuir* **1991**, *7*, 2438.
(29) O'Neil, G. A.; Torkelson, J. M. *Macromolecules* **1997**, *30*, 5560.
(30) Farinba, J. P. S.; Vorobyova, O.; Winnik, M. A. *Macromolecules* **2000**, *33*, 5863.
(31) Ohshima, A.; Yamagata, A.; Sato, T.; Teramoto, A. *Macromolecules* **1999**, *32*, 8645.
(32) Dlubek, G.; Pionteck, J.; Bondarenko, V.; Pompe, G.; Taesler, Ch.; Petters, K.; Krause-Rehberg, R. *Macromolecules* **2002**, *35*, 6313.
(33) Wang, S.; von Meerwall, E. D.; Wang, S.; Halasa, A.; Hsu, W. L.; Zhou, J. P.; Quirk, R. P. *Macromolecules* **2004**, *37*, 1641.
(34) Price, K. E.; Broadwater, S. J.; Bogdan, A. R.; Keresztes, I.; Steinbacher, J. L.; McQuade, D. T. *Macromolecules* **2006**, *39*, 7681.
(35) High, M. S.; Painter, P. C.; Coleman, M. M. *Macromolecules* **1992**, *25*, 797.
(36) Van Alsten, J. G.; Lustig, S. R. *Macromolecules* **1992**, *25*, 5069.
(37) Jabbari, E.; Peppas, N. A. *Macromolecules* **1993**, *26*, 2175.
(38) Tomba, J. P.; Carella, J. M.; Garcia, D.; Pastor, J. M. *Macromolecules* **2001**, *34*, 2277.
(39) Tomba, J. P.; Carrela, J. M.; Garcia, D.; Pastor, J. M. *Macromolecules* **2004**, *37*, 4940.
(40) Arzondo, L.; Tomba, J. P.; Carrella, J. M.; Pastor, J. M. *Macromol. Rapid Commun.* **2005**, *26*, 632.
(41) Tomba, J. P.; Carrela, J. M.; Parstor, J. M.; Fernández, M. R. *Macromol. Rapid Commun.* **1998**, *19*, 413.

(42) Lin, H. C.; Tsai, I. F.; Yang, A. C.-M.; Hsu, M. S.; Ling, Y. C. *Macromolecules* **2003**, *36*, 2464.
(43) Schaffer, M.; Janarthanan, V.; Deng, Y.; La Scala, J.; Guo, L.; Rafailovich, M.; Sokolov, J.; Stein, R. S.; Strzhemechny, Y.; Schwarz, S. A. *Macromolecules* **1997**, *30*, 1225.
(44) Zheng, X.; Rafailovich, M. H.; Sokolov, J.; Strzhemechny, Y.; Schwarz, S. A.; Sauer, B. B.; Rubinstein, M. *Phys. Rev. Lett.* **1997**, *79*, 241.
(45) Harton, S. E.; Stevie, F. A.; Ade, H. *Macromolecules* **2005**, *38*, 3543.
(46) Whitlow, S.; Wool, R. P. *Macromolecules* **1991**, *24*, 5926.
(47) Zheng, X.; Rafailovich, M. H.; Sokolov, J.; Zhao, X.; Briber, R. M.; Schwarz, S. A. *Macromolecules* **1993**, *26*, 6431.
(48) Siangchaew, K.; Libera, M. *Macromolecules* **1999**, *32*, 3051.
(49) Parker, M. A.; Vesely, D. *J. Polym. Sci., Polym. Phys.* **1986**, *24*, 1869.
(50) Horiuchi, S.; Dohi, H. *Langmuir* **2006**, *22*, 4607.
(51) Liao, Y. G.; Horiuchi, S.; Nunoshige, J.; Akahoshi, H.; Ueda, M. *Polymer* **2007**, *48*, 3749.
(52) Plivelic, T. S.; Cassu, S. N.; do Carmo Goncalves, M.; Torriani, I. L. *Macromolecules* **2007**, *40*, 253.
(53) Horiuchi, S.; Yin, D. H.; Liao, Y. G.; Ougizawa, T. *Macromol. Rapid Commun.* **2007**, *28*, 915.
(54) Creton, C.; Kramer, E. J.; Hui, C. Y.; Brown, H. R. *Macromolecules* **1992**, *25*, 3075.
(55) Janarthanan, V.; Stein, R. S.; Garret, P. D. *Macromolecules* **1994**, *27*, 4855.
(56) Cole, P. J.; Cook, R. F.; Macosko, C. W. *Macromolecules* **2003**, *36*, 2808.
(57) Dohi, H.; Horiuchi, S. *Polymer* **2007**, *48*, 2526.
(58) Horiuchi, S.; Fujita, T.; Hayakawa, T.; Nakao, Y. *Langmuir* **2003**, *19*, 2963.
(59) Horiuchi, S.; Yin, D. H.; Ougizawa, T. *Macromol. Chem. Phys.* **2005**, *206*, 725.
(60) Ten Brinke, G.; Karasz, F. E.; MacKnight, W. J. *Macromolecules* **1983**, *16*, 1827.
(61) Rouse, P. E. *J. Chem. Phys.* **1953**, *21*, 1272.
(62) Brown, H. R. *Macromolecules* **2001**, *34*, 3720.
(63) Schnell, R.; Stamm, M.; Creton, C. *Macromolecules* **1998**, *31*, 2284.

MA071535G